GEOPHYSICAL RESEARCH LETTERS, VOL. 34, L02305, doi:10.1029/2006GL028586, 2007

3-D surface wave tomography of the Piton de la Fournaise volcano using seismic noise correlations

Florent Brenguier,[1,2] Nikolai M. Shapiro,[2] Michel Campillo,[1] Alexandre Nercessian,[2] and Valérie Ferrazzini[3]

Received 26 October 2006; revised 29 November 2006; accepted 7 December 2006; published 26 January 2007.

[1] We invert Rayleigh waves reconstructed from cross-correlations of 18 months of ambient seismic noise recorded by permanent seismological stations run by the Piton de la Fournaise Volcanological Observatory. By correlating noise records between 21 receivers, we reconstruct Rayleigh waves with sufficient signal-to-noise ratio for 210 inter-station paths. We use the reconstructed waveforms to measure group velocity dispersion curves at periods between 1.5 and 4.5 s. The obtained measurements are inverted for two-dimensional group velocity maps and finally for a 3-D S-wave velocity model of the edifice from +2 to −1 km above sea level. Our results clearly show a high velocity body spatially delimited by the borders of the active 10 km wide caldera. The preferential N30°-N130° orientations of this anomaly at −0.5 km below sea-level is an evidence of the preferential paths of magma injections associated to the NE-SE Rift Zones. This structure is surrounded by a low-velocity ring interpreted as effusive products associated to the construction of the Piton de la Fournaise volcano on the flank of the older Piton des Neiges volcano. **Citation:** Brenguier, F., N. M. Shapiro, M. Campillo, A. Nercessian, and V. Ferrazzini (2007), 3-D surface wave tomography of the Piton de la Fournaise volcano using seismic noise correlations, *Geophys. Res. Lett.*, *34*, L02305, doi:10.1029/2006GL028586.

1. Introduction

[2] Piton de la Fournaise is a basaltic volcano located on the eastern side of *La Réunion* island, in the Indian Ocean. Piton de la Fournaise is one of the most active volcanoes in the world. During the past two centuries its average time between consecutive eruptions was about 10 months [*Stieltjes and Moutou*, 1989]. The 2600 m high and 10 km wide active caldera is characterized by two main radial fracture zones in the directions north 170° and 10° [*Bachélery*, 1981] (Figure 1a). Those fracture zones are interpreted as active rift zones. However, previous tomographic studies did not show evidence of the rift zone extensions at depth [*Nercessian et al.*, 1996].

[3] In the last decade, seismic tomographies on volcanoes have provided structural images with an increasing resolution [e.g., *Zollo et al.*, 2002; *Tanaka et al.*, 2002; *Yamawaki et al.*, 2004; *Brenguier et al.*, 2006]. For most of these studies, the objective is either to determine the velocity structure of the entire volcano, or to map details such as possible location of melt material, shallow magma reservoir, or heterogeneities that correlate with seismic activity [*Kodaira et al.*, 2002]. These experiments have an horizontal extent of 10 to 20 km, a depth of investigation of a few km, and a spatial resolution of the order of few km. However, these studies are hampered by irregular distribution of sources (earthquakes or active sources).

[4] These studies are commonly based on the inversion of P first arrival times and thus do not provide consistent S wave velocity model of the studied structure. The Vp/Vs ratio however appears to be a reliable criterion to assess for the presence of fluid (hydrothermal circulation, magma ascent)[*Laigle et al.*, 2000]. The inversion of surface waves in volcanic domain from array analysis leads to Vs velocity models but suffers from the dependency to the nature of volcanic sources [*Ferrazzini et al.*, 1991; *Saccorotti et al.*, 2003].

[5] In the field of ultrasonics, it has been shown both theoretically and experimentally that a random wavefield has correlations which, on average, take the form of the Green's function of the media [*Weaver and Lobkis*, 2001; *Lobkis and Weaver*, 2001]. In seismology, recent studies also showed that the Rayleigh wave Green's function between pairs of seismographs can be extracted from cross-correlations of coda waves and ambient noise [*Shapiro and Campillo*, 2004; [*Campillo*, 2006]. Moreover, some authors used correlations of long ambient seismic noise sequences from regional networks in order to extract and to invert Rayleigh waves to produce high-resolution seismic images of the shallow crustal layers under these networks [*Shapiro et al.*, 2005; *Sabra et al.*, 2005; *Kang and Shin*, 2006].

[6] We propose, in this paper, to estimate a 3-D S-wave velocity model of the Piton de la Fournaise volcano. We apply the technique of ambient noise cross correlations to retrieve the Rayleigh wave Green's functions between each pair of seismographs. We use the reconstructed waveforms to measure group velocity dispersion curves and to obtain two-dimensional group velocity maps by tomography. We finally invert these maps for a 3-D S-wave velocity model of the edifice from +2 to −1 km above sea level.

2. Data Processing

[7] We collected 18 months (Jul. 1999 to Dec. 2000) of continuous seismic noise recorded from the 21 vertical short period stations ran by the Observatoire Volcanologique du Piton de la Fournaise (Figure 1a). One of the advantages of this network is that all stations use the same equipment

[1]Laboratoire de Géophysique Interne et Tectonophysique, CNRS, Université Joseph Fourier, Grenoble, France.
[2]Institut de Physique du Globe de Paris, CNRS, Paris, France.
[3]Observatoire Volcanologique du Piton de la Fournaise, Institut de Physique du Globe de Paris, Réunion, France.

0094-8276/07/2006GL028586$05.00

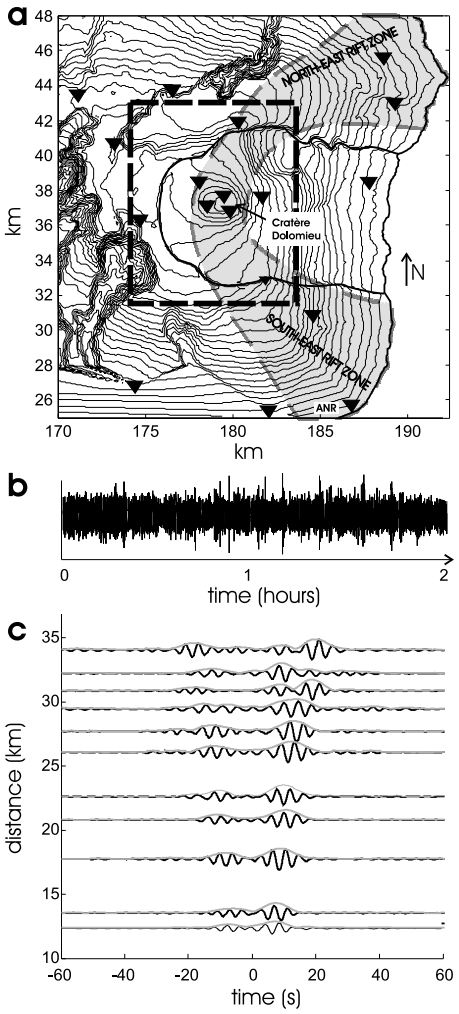

Figure 1. (a) Map of the Piton de la Fournaise volcano. Seismic stations are represented as inverted triangles. The gray zone indicates the limits of the rift zone. The thick dashed rectangle corresponds to the limits of the presented tomographic images. Geographic coordinates are Gauss-Laborde kilometric coordinates (Transverse Mercator). Contour lines are spaced every 100 m. (b) Two hours of ambient seismic noise (ANR). (c) Causal and acausal reconstructed Rayleigh waves (positive and negative times; dominant period, 4 s) between station RMR (not shown on the map) and the rest of the network. The trace envelopes are represented as thin gray curves.

(available at http://www.ipgp.jussieu.fr/pages/030308.php). This allows us to make inter-stations measurements without dealing with the problem of the instrumental corrections. An example of a noise record at one of the stations (ANR) is shown in Figure 1b. We first filter the data between 1 to 5 s and whiten their spectral amplitude in order to avoid dominance of strong spectral peaks in the noise. We further normalize the data by disregarding completely the amplitudes and by keeping only a one-bit signal [*Campillo and Paul*, 2003]. This procedure is necessary in order to avoid the dominance, in the correlations, of energetic arrivals such as earthquake signal or storms. Data corresponding to one day are cross-correlated for each station pair. We then reject traces according to a signal to noise ratio criterion (24% rejection on average) and stack the non-rejected traces day per day over 18 months (540 days). An example of reconstructed Rayleigh waves is shown in Figure 1c.

[8] We then estimate a group velocity dispersion curve for each stacked trace using an automatic Frequency-Time Analysis (FTAN) [*Levshin et al.*, 1989; *Ritzwoller and Levshin*, 1998]. We manually select the dispersion curves (DP) according to group velocity limits (50% variation around an average DP) and such that the station-to-station distance be longer than one wavelength. We finally obtain 75 reliable dispersion curves and extract group velocities for each trace for periods equal to 2, 2.5, 3, 3.5, 4, and 4.5 s (Figure 2a).

3. Rayleigh Wave Tomography

[9] We perform a tomographic inversion of the arrival-time measurements deduced from the group velocity measurements at each period using the algorithm described by [*Barmin et al.*, 2001]. The regularization scheme of this

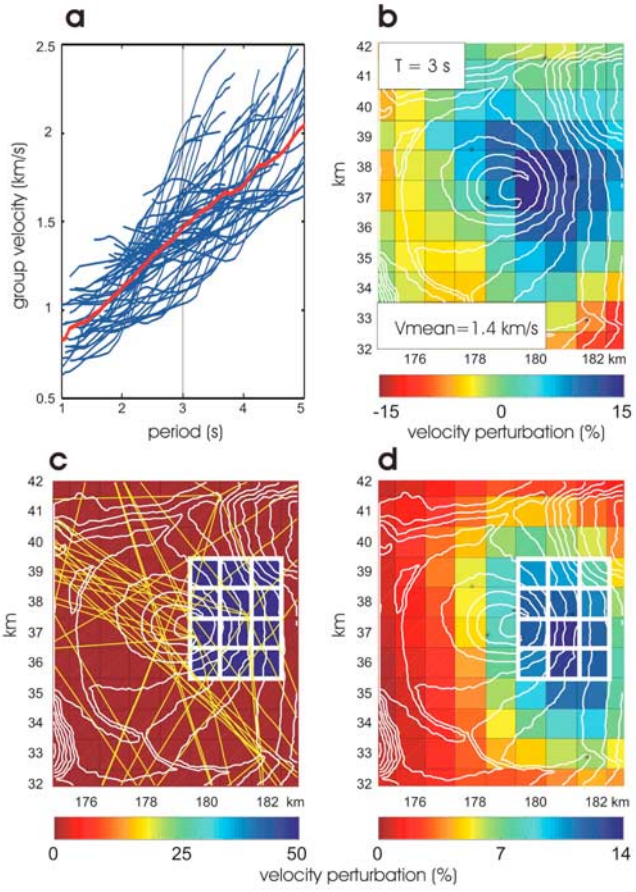

Figure 2. (a) Seventy-five selected dispersion curves used for tomography. The average dispersion curve is represented by a red line. (b) Three-second Rayleigh-wave group-velocity map. Topography is represented as white contour lines. (c) Input synthetic velocity model for the spike test. The spike mesh is plotted as thick white lines. Rays are represented as yellow lines (real-case ray distribution). The 0% perturbation corresponds to a velocity of 1.5 km/s. (d) Results of inversion of the synthetic data.

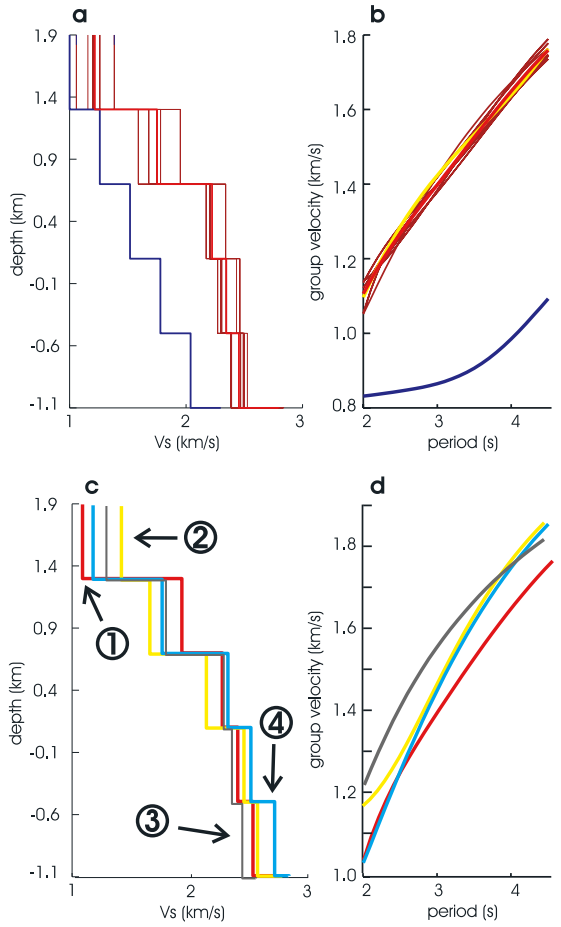

Figure 3. (a) Inverted velocity profiles for one cell (near point 1 on Figure 4). The blue line is the initial velocity profile. The 10 thin and the thick red lines are 10 best fitting velocity profiles (whose associated dispersion curves (DC) best fit the measured DC) and their average. (b) The blue line is the DC associated to the initial velocity profile. The yellow thick line is the measured DC. The 10 thin and the thick red lines are respectively, the 10 best fitting DC and their average. (c) Different average velocity profiles obtained from the inversion at different cells, and (d) their associated calculated DC. Their positions are shown on Figure 4.

method involves a penalty function composed of a spatial smoothing function and a constraint on the amplitude of the perturbation depending on local path density. Our 2-D model involves $22 \times 28 = 616$ 1×1 km cells. The initial velocity is taken as the average of the group velocity measurements at each period. We do not take into account the topography during the inversion procedure. This approximation yields an error <5% on group velocity measurements. However, the group velocity measurements show variations of more than 50% at a each period (Figure 2a). The error caused by the flat topography approximation is, therefore, negligible.

[10] Because of the sparse ray coverage and the low resolution of the data set, we chose to apply a strong smoothing during the tomographic inversion. The spatial resolution (≈4 km) is constrained by the smoothing condition. The inversion results are thus robust and show a moderate variance reduction varying from 38 to 18% with increasing periods (from 2 to 4.5 s).

[11] Estimated distribution of Rayleigh wave group velocities at 3 s is shown in Figure 2b within the zone where the model is best resolved. The tomographic image clearly shows a high velocity anomaly 1 km east of the main vent (cratre Dolomieu, Figure 1). We perform a spike test in order to test how well this high velocity anomaly is resolved. The true velocity model is taken as a 3×4 km wide high velocity anomaly (Figure 2c). The inversion of the synthetic data shows that the anomaly is well located but its shape is highly smoothed and characterized by a North-West South-East trend due to the similar preferential orientation of rays (Figure 2d). Moreover, the amplitude of the anomaly is attenuated by a factor 3 due to the smoothing condition.

4. Depth Inversion

[12] We construct dispersion curves for each model cell from the tomographic maps corresponding to periods 2, 2.5, 3, 3.5, 4, and 4.5 s. We fit these curves by polynomial functions in a least-squares sense and invert them using a Monte-Carlo algorithm [*Shapiro et al.*, 1997], the synthetic dispersion curve being calculated using a method by [*Herrmann and Al-Eqabi*, 1991]. We thus obtain a Vs versus depth velocity profile for each cell. Figures 3a and 3b show depth inversion results of one dispersion curve. Figure 3a illustrates the non-uniqueness of the velocity structures determined by dispersion curve inversion. We average 10 best fitting models for each cell and spatially smooth the 3-D reconstructed velocity model in order to retrieve the average subsurface velocity distribution. Figures 3c and 3d show different velocity profiles corresponding to a near-surface low velocity anomaly (curve 1), a near-surface high velocity anomaly (curve 2), a 1 km below sea level (bsl) low velocity anomaly (curve 3), and a 1 km bsl high velocity anomaly (curve 4). The horizontal location of these profiles is shown on Figure 4.

[13] We present 6 horizontal slices as well as a 3-D view of the 3-D smoothed model on Figure 4. The results clearly show the presence of a high velocity anomaly which moves westward with depth (+1.3 to −1.1 km above sea level). This structure is surrounded by a low-velocity ring interpreted as effusive products associated to the construction of the Piton de la Fournaise volcano on the flank of the older Piton des Neiges volcano. This high velocity anomaly has also been detected by a previous earthquake and active P-wave tomography on the Piton de la Fournaise volcano [*Lankar*, 1997]. Recent works also imaged the presence of a high velocity chimney on different volcanoes [*Laigle et al.*, 2000; *Tanaka et al.*, 2002; *Zollo et al.*, 2002; *Sherburn et al.*, 2006; *Patanè et al.*, 2006]. We interpret this anomaly as a solidified intrusive magma body. The high velocity anomaly is also well correlated with the rift zone at sea level (Z = −0.5 km).

5. Discussion and Conclusions

[14] We used 18 months of seismic noise recorded by the seismological network of the Piton de la Fournaise volcano

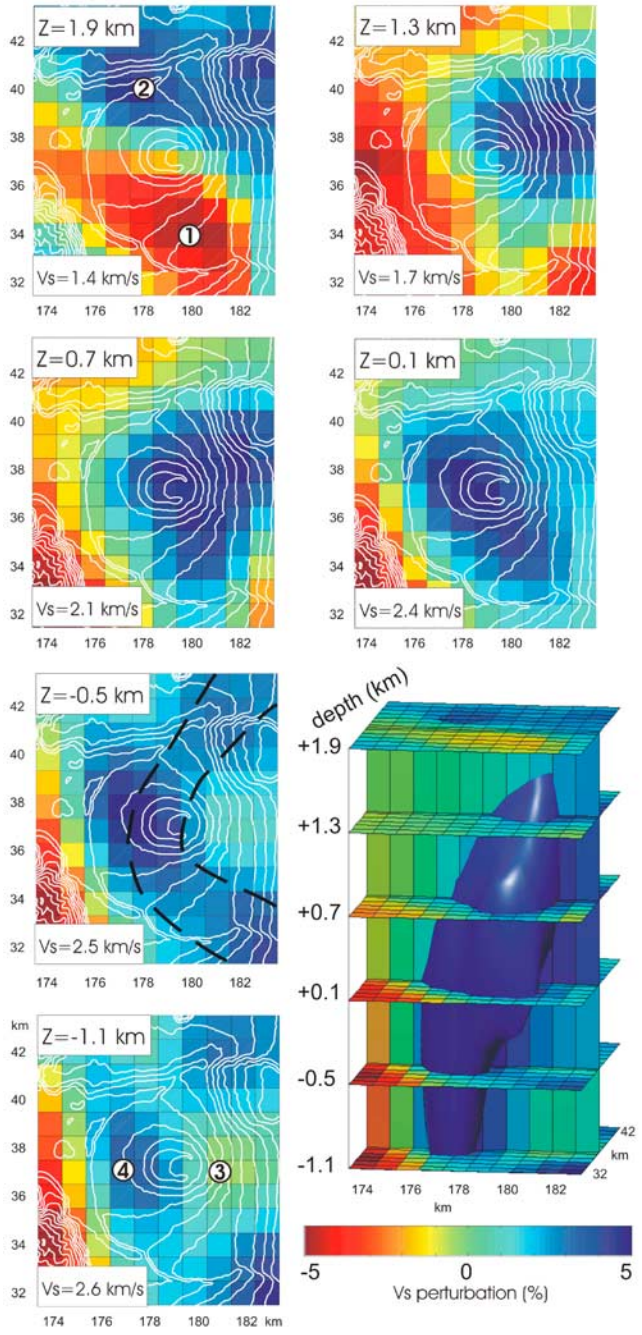

Figure 4. 3-D S-wave velocity model. We show 6 horizontal slices extracted from the 3-D model at different depths. Average S-wave velocity is shown in white boxes on the bottom of corresponding slices. Black dashed line at depth -0.5 km shows the limits of the rift zone. We also plot a 3-D view of the model. The 3-D blue patch delimits the iso-velocity perturbation surface corresponding to 2.5% of velocity perturbation. The circled numbers show the horizontal positions of the vertical velocity profiles shown in Figure 3c.

to reconstruct Rayleigh wave Green's functions between each pair of seismic sensors. We used these waveforms to perform a Rayleigh-wave tomography and invert dispersion curves extracted from group velocity maps in order to build a 3-D S-wave velocity model of the 10 km width active caldera from +2 to −1 km above sea level.

[15] Our approach relies on a strong quality selection of the data. We apply a strong smoothing condition on our tomographic models to increase the robustness of the inversion. This condition, however, limits the spatial resolution and leads to strongly underestimated amplitudes of the inferred seismic speed anomalies. Our method results in a better resolution in shallow layers than earthquake-based tomographies because it is not limited by the spatial repartition of sources within the volcano that provides with only a very limited number of near-surface paths.

[16] Our results agree with earthquake and active P-wave tomographies previously performed on this edifice [*Lankar*, 1997] showing an intrusive high velocity body moving westward from the surface to 1 km below sea level. Imaging these intrusive bodies is of particular interest because the magma path is usually believed to follow their geometry [*Laigle et al.*, 2000; *Battaglia et al.*, 2005].

[17] This work validates a new technique of 3-D surface waves tomography using correlations of ambient seismic noise. Moreover, we performed a preliminary study showing that, with this data set, using only a few instead of 18 months of seismic noise records will yield similar tomographic results. This method is thus particularly advantageous in the context of temporary seismic arrays because it can return useful information of the near-surface structure even if earthquakes do not occur. This method may also be complementary to prohibitively expensive active seismic source tomography.

[18] **Acknowledgments.** All the data used in this work were collected by the seismological network of the Observatoire Volcanologique du Piton de la Fournaise. We are grateful to the Observatory staff and also to Zacharie Duputel and Luis Rivera for the help with the data. We thank Laurent Stehly, Pierre Gouédard, and Philippe Roux (LGIT) for helpful discussions. We thank Alfred Hirn (IPGP) for discussions about the Piton de la Fournaise P-wave tomography. We are grateful to Olivier Coutant, Jean-Robert Grasso, Kees Wapenaar, and Tae-Seob Kang for constructive comments concerning the manuscript. This work was supported by ANR (France) under contracts 05-CATT-010-01 (PRECORSIS) and COHERSIS.

References

Bachélery, P. (1981), Le Piton de la Fournaise (Ile de la Réunion): Etude volcanologique, structurale et pétrologique, thesis, Univ. Blaise Pascal, Clermont-Ferrand, France.

Barmin, M. P., M. H. Ritzwoller, and A. L. Levshin (2001), A fast and reliable method for surface wave tomography, *Pure Appl. Geophys.*, *158*, 1351–1375.

Battaglia, J., V. Ferrazzini, T. Staudacher, K. Aki, and J.-L. Cheminée (2005), Pre-eruptive migration of earthquakes at the Piton de la Fournaise volcano (Réunion Island), *Geophys. J. Int.*, *161*, 449–458.

Brenguier, F., O. Coutant, H. Baudon, F. Doré, and M. Dietrich (2006), High resolution seismic tomography of a Strombolian volcanic cone, *Geophys. Res. Lett.*, *33*, L16314, doi:10.1029/2006GL026902.

Campillo, M. (2006), Phase and correlation in random seismic fields and the reconstruction of the Green function, *Pure Appl. Geophys.*, *163*, 475–502.

Campillo, M., and A. Paul (2003), Long-range correlations in the diffuse seismic coda, *Science*, *299*, 547–549.

Ferrazzini, V., K. Aki, and B. Chouet (1991), Characteristics of seismic waves composing Hawaiian volcanic tremor and gas-piston events observed by a near-source array, *J. Geophys. Res.*, *96*, 148–227.

Herrmann, R. B., and G. Al-Eqabi (1991), Surface waves: Inversion for shear wave velocity, in *Shear Waves in Marine Sediments*, edited by J. M. Hovem, M. D. Richardson, and R. D. Stoll, pp. 545–556, Springer, New York.

Kang, T.-S., and J. S. Shin (2006), Surface-wave tomography from ambient seismic noise of accelerograph networks in southern Korea, *Geophys. Res. Lett.*, *33*, L17303, doi:10.1029/2006GL027044.

Kodaira, S., K. Uhira, T. Tsuru, H. Sugioka, K. Suyehiro, and Y. Kaneda (2002), Seismic image and its implications for an earthquake swarm at an active volcanic region off the Miyake-jima–Kozu-shima, Japan, *Geophys. Res. Lett.*, *29*(11), 1548, doi:10.1029/2001GL014377.

Laigle, M., A. Hirn, M. Sapin, J.-C. Lépine, J. Diaz, J. Gallart, and R. Nicolich (2000), Mount Etna dense array local earthquake *P* and *S* tomography and implications for volcanic plumbing, *J. Geophys. Res.*, *105*, 21,633–21,646.

Lankar, V. (1997), Approches par tomographie sismique du Piton de la Fournaise, La Réunion, thesis, Inst. de Phys. du Globe, Paris.

Levshin, A. L., T. B. Yanocskaya, A. V. Lander, B. G. Bukchin, M. P. Barmin, L. I. Ratnikova, and E. N. Its (1989), *Seismic Surface Waves in a Laterally Inhomogeneous Earth*, edited by V. I. Keilis-Borok, Springer, New York.

Lobkis, O. I., and R. Weaver (2001), On the emergence of the Green's function in the correlations of a diffuse field, *J. Acoust. Soc. Am.*, *110*(6), 3011–3017.

Nercessian, A., A. Hirn, J.-C. Lépine, and M. Sapin (1996), Internal structure of Piton de la Fournaise volcano from seismic wave propagation and earthquake distribution, *J. Volcanol. Geotherm. Res.*, *70*, 123–143.

Patané, D., G. Barberi, O. Cocina, P. De Gori, and C. Chiarabba (2006), Time-resolved seismic tomography detects magma intrusions at Mount Etna, *Science*, *313*, 821–823.

Ritzwoller, M., and A. L. Levshin (1998), Eurasian surface wave tomography: Group velocities, *J. Geophys. Res.*, *103*, 4839–4878.

Sabra, K. G., P. Gerstoft, P. Roux, W. A. Kuperman, and M. C. Fehler (2005), Surface wave tomography from microseisms in southern California, *Geophys. Res. Lett.*, *32*, L14311, doi:10.1029/2005GL023155.

Saccorotti, G., B. Chouet, and P. Dawson (2003), Shallow-velocity models at the Kilauea volcano, Hawaii, determined from array analyses of tremor wavefields, *Geophys. J. Int.*, *152*, 633–648.

Shapiro, N. M., and M. Campillo (2004), Emergence of broadband Rayleigh waves from correlations of the ambient seismic noise, *Geophys. Res. Lett.*, *31*, L07614, doi:10.1029/2004GL019491.

Shapiro, N. M., M. Campillo, A. Paul, S. K. Singh, D. Jongmans, and F. J. Sanchez-Sesma (1997), Surface-wave propagation across the Mexican volcanic belt and the origin of the long-period seismic-wave amplification in the Valley of Mexico, *Geophys. J. Int.*, *128*, 151–166.

Shapiro, N. M., M. Campillo, L. Stehly, and M. H. Ritzwoller (2005), High-resolution surface-wave tomography from ambient seismic noise, *Science*, *307*, 1615–1618.

Sherburn, S., R. S. White, and M. Chadwick (2006), Three-dimensional tomographic imaging of the Taranaki volcanoes, New Zealand, *Geophys. J. Int.*, *166*, 957–969.

Stieltjes, L., and P. Moutou (1989), A statistical and probabilistic study of the historic activity of the Piton de la Fournaise, Réunion Island, Indian Ocean, *J. Volcanol. Geotherm. Res.*, *36*, 67–86.

Tanaka, S., et al. (2002), Three-dimensional *P*-wave velocity structure of Iwate volcano, Japan, from active seismic survey, *Geophys. Res. Lett.*, *29*(10), 1420, doi:10.1029/2002GL014983.

Weaver, R. L., and O. I. Lobkis (2001), Ultrasonics without a source: Thermal fluctuation correlations at MHz frequencies, *Phys. Rev. Lett.*, *87*(13), doi:10.1103/PhysRevLett.87.134301.

Yamawaki, T., et al. (2004), Three-dimensional *P*-wave velocity structure of Bandai volcano in northeastern Japan inferred from active seismic survey, *J. Volcanol. Geotherm. Res.*, *138*, 267–282.

Zollo, A., L. D'Auria, R. D. Matteis, A. Herrero, J. Virieux, and P. Gasparini (2002), Bayesian estimation of 2-D *P*-velocity models from active seismic arrival time data: Imaging of the shallow structure of Mt. Vesuvius, *Geophys. J. Int.*, *151*, 566–582.

F. Brenguier and M. Campillo, Laboratoire de Géophysique Interne et Tectonophysique, CNRS, BP 53, F-38041 Grenoble, France. (florent.brenguier@ujf-grenoble.fr)

V. Ferrazzini, Observatoire Volcanologique du Piton de la Fournaise, IPGP, 14 RN3, Km 27, F-97418 Réunion, France.

A. Nercessian and N. M. Shapiro, Institut de Physique du Globe de Paris, CNRS, 4 place Jussieu, F-75252 Paris, France.